

Error Semitransparent Universal Control of a Bosonic Logical Qubit

Saswata Roy,^{1,*} Owen C. Wetherbee,^{1,2} and Valla Fatemi^{3,†}

¹*Department of Physics, Cornell University, Ithaca, NY, 14853, USA*

²*Department of Physics, University of California, Berkeley, USA*

³*School of Applied and Engineering Physics,
Cornell University, Ithaca, NY, 14853, USA*

Abstract

Bosonic codes offer hardware-efficient approaches to logical qubit construction and hosted the first demonstration of beyond-break even logical quantum memory. However, such accomplishments were done for idling information, and realization of fault-tolerant logical operations remains a critical bottleneck for universal quantum computation in scaled systems. Error-transparent (ET) gates offer an avenue to resolve this issue, but experimental demonstrations have been limited to phase gates. Here, we introduce a framework based on dynamic encoding subspaces that enables simple linear drives to accomplish universal gates that are error semi-transparent (EsT) to oscillator photon loss. With an EsT logical gate set of $\{X, H, T\}$, we observe a five-fold reduction in infidelity conditioned on photon loss, demonstrate extended active-manipulation lifetimes with quantum error correction, and construct a composite EsT non-Clifford operation using a sequence of eight gates from the set. Our approach is compatible with methods for detectable ancilla errors, offering an approach to error-mitigated universal control of bosonic logical qubits with the standard quantum control toolkit.

I. INTRODUCTION

Realization of quantum computation faces the challenge of noise destroying encoded quantum information. Quantum error correction (QEC) can tackle this problem by encoding logical quantum information with redundancy to correct physical errors. Recent experiments demonstrated implementation of QEC to protect stored logical quantum information in large arrays of physical qubits [1–3] and in single harmonic oscillators [4–10]. The latter approach, in which bosonic codes take advantage of the large Hilbert space of a harmonic oscillator, has emerged as a leading platform for hardware-efficient quantum information processing [11–13] with multiple experiments crossing the break even point [4–9].

Realized experiments focus on logical qubits that are protected from errors while the qubit is idling. Fault-tolerant quantum computing also requires fault-tolerant processing of quantum information. In arrays of physical qubits, this is accomplished via a set of transversal gates and magic states [14]. For bosonic codes, the Hilbert space is not as easily separable, so the more general formalism of error transparent (ET) gates [15, 16] or path-independent gates [17, 18] provides a path to fault-tolerant manipulation. The fault-tolerance can be towards the errors of the oscillator and/or the ancilla. In particular, ET gates are designed to have similar trajectories in code and error subspaces within the large Hilbert space. Experiments demonstrated ET [19] and path-independent [20] gates for phase gates in binomial logical qubits. However, universal quantum computation requires implementation of amplitude mixing gates such as the X or H gates. While conventional (non-ET) universal control was accomplished in Ref. [10], realization of ET universal control remains

an outstanding challenge.

Theoretically, the implementation of amplitude mixing ET gates using non-linear drives has been proposed [19, 21]. These operations achieve error transparency by matching the phase and trajectory of the evolution of the code and error subspaces while staying entirely within the static code and error subspaces. However, this approach presents significant experimental challenges due to the requirement of particularly strong nonlinear drives and extremely strict confinement to the static logical spaces, which are not currently natural or high-fidelity approaches for oscillator control [22, 23].

Here, we propose considering dynamic code and error subspaces as a framework to relax the static codespace requirements for error transparency. This allows us to achieve error semi-transparent (EsT) operations using only linear drives on both the oscillator and ancilla, which is the standard optimal control ‘toolkit’ for circuit quantum electrodynamics (cQED) [24–26]. These simpler controls also ensure fast gates, high reliability, and fewer spurious parametric processes that can complicate the dynamics. The drawback is that, formally, exact error transparency for oscillator photon loss, the primary source of loss for bosonic codes, cannot be achieved because linear drive Hamiltonians cannot strictly commute with the photon loss errors on the codespace. Nonetheless, this tradeoff can be explored for obtaining error correction gain for *actively controlled* logical quantum information.

Using pulses numerically optimized for dynamic subspace error transparency to bosonic photon loss, we experimentally demonstrate universal control of a binomial logical qubit with X , H and T gates. We compare the performance with that of ordinary, non-ET gates (henceforth named Ord gates), finding that EsT gates enhance performance in presence of photon loss errors occurring during gate operations. We observe an average factor of five reduction in logical infidelity for the actively controlled logical states conditioned on a photon loss event

* sr938@cornell.edu

† vf82@cornell.edu

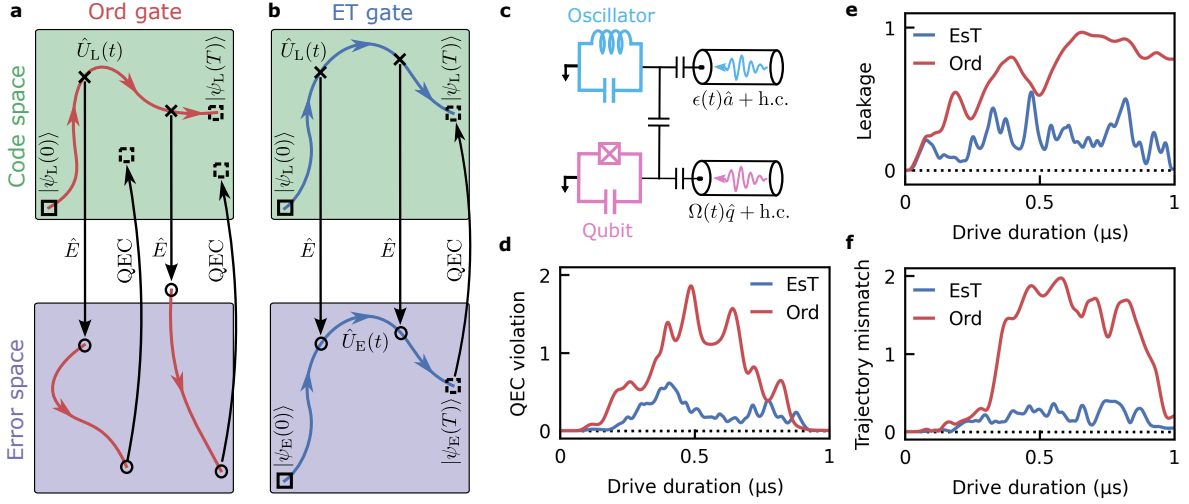


FIG. 1. **Concept and operation of ET gate:** During a logical operation $U_L(t)$ that takes the logical code space state $|\psi_L(0)\rangle$ at time $t = 0$ to $|\psi_L(T)\rangle$ at time $t = T$, an error may occur at any time t , taking the state from code space to an orthogonal error space. (a) For an ordinary gate, an error at any point destroys the effect of the operation in the error space. Importantly, the final state depends on the exact time of the error occurring, which is a probabilistic event. (b) For an ET operation the trajectories in error and code space are identical. Hence an error happening at any time takes the state through a deterministic path in error space and ends at the same final state preserving the effect of the gate in error space. Therefore a quantum error correction (QEC) process can be used to detect and correct the error at the end of the operation, making the ET operation tolerant of errors during it. (c) An ancilla transmon qubit and an oscillator coupled to it are driven with numerically optimized pulses for realization of ET operations on an encoded logical qubit in the oscillator. (d) QEC violation for the evolved code space basis states during a logical X operation on a binomial logical qubit encoded in the oscillator. Numerically optimized EsT gate has minimal violation compared to the Ord gate. (e) Leakage out of the instantaneous error space and (f) trajectory mismatch in code and error subspaces also show smaller violation for EsT gate compared to Ord gate. Violation metrics plotted in (e) and (f) are calculated for an initial state $|0_E\rangle$ and $|0_L\rangle$, respectively.

during the gate. Commensurately, the EsT gates perform significantly better than the Ord gate after applying error correction following the operation. Further, we show that distinct gates from the set are compatible for digital construction of arbitrary unitary operations [27, 28] while preserving the EsT property.

II. THEORETICAL CONCEPT

We begin by defining ideal ET operations. As described in Ref. [15, 16, 19], a logical unitary U is ET if it commutes with the error set $\{E_j\}$ throughout the operation, such that $U(T, t)E_jU(t, 0)|\psi_L(0)\rangle = e^{i\phi_j(t)}E_jU(T, 0)|\psi_L(0)\rangle$, $\forall j, t, |\psi_L(0)\rangle$, where $U(t_2, t_1)$ describes the unitary operation from time t_1 to t_2 , T is the final time such that $U = U(T, 0)$, $\phi_j(t)$ is a global phase, and $|\psi_L(0)\rangle$ denotes a state in the code space at time $t = 0$. If the code and error spaces are static, meaning $U(t, 0)$ remains a logical unitary for all t , this ET condition can be satisfied by engineering the Hamiltonian to act identically within the code and error spaces: $P_j^\dagger H(t)P_j = P_C^\dagger H(t)P_C + d_j(t)P_C$, $\forall j, t$, where, $P_j \propto E_jP_C$ is the projector from the code space to the error space corresponding to the error E_j , P_C is the codespace projector and $d_j(t)$ is a complex number.

To relax the requirement of static code and error spaces,

we propose defining an instantaneous codespace

$$\mathcal{C}(t) = \{U(t, 0)|\psi_L(0)\rangle \mid |\psi_L(0)\rangle \in \mathcal{C}(0)\}, \quad (1)$$

with instantaneous projectors $P_C(t) = U(t, 0)P_CU^\dagger(t, 0)$. We can define a corresponding instantaneous error space ($\mathcal{E}_j(t)$) as

$$\mathcal{E}_j(t) = \text{span}\{E_j|\psi_L(t)\rangle \mid |\psi_L(t)\rangle \in \mathcal{C}(t)\}, \quad (2)$$

with projector $P_{\mathcal{E}_j}(t) \propto E_jP_C(t)E_j^\dagger$. Then we need to enforce three conditions on our engineered dynamics for error transparency.

First, the instantaneous code space must remain valid and correctable at all times, satisfying the QEC conditions (Knill-Laflamme conditions) throughout the trajectory. For a general error set $\{E_k\}$, this requires that the projection of all error products into the instantaneous code space is proportional to the logical identity:

$$P_C(t)E_i^\dagger E_j P_C(t) = c_{ij}(t)P_C(t), \quad \forall i, j, \quad (3)$$

where $c_{ij}(t)$ are complex coefficients.

Second, the evolved error space under the application of the unitary should coincide with the instantaneous error space defined above. This can be written as

$$U(t, 0)\mathcal{E}_j(0) = \mathcal{E}_j(t), \quad \forall j, t, \quad (4)$$

Third, the Hamiltonian must drive identical dynamics within these instantaneous code and error subspaces:

$$P_j^\dagger(t)H(t)P_j(t) = P_C^\dagger(t)H(t)P_C(t) + d_j(t)P_C(t), \forall j, t, \quad (5)$$

where $d_j(t)$ is a time-dependent complex number. Fulfilling these three conditions in the dynamic subspaces, the ET property can in principle be maintained throughout the operation.

To quantify the deviation from ideal ET in our dynamic subspaces, we introduce three time-dependent metrics: QEC violation, instantaneous leakage and trajectory mismatch. Here we will define them analytically, and later we will assess the measures for the gates derived for our particular setup.

To evaluate deviations from ideal instantaneous correctability, we define the QEC violation metric, $\Delta_{\text{QEC}}(t)$ [29] (see App. A for details). Assuming a two-dimensional logical subspace, we define the 2×2 projected error matrices as $M_{ik}(t) = P_C(t)E_i^\dagger E_k P_C(t)$. From this matrix $M_{ik}(t)$, the QEC violation metric isolates and sums the magnitude of the uncorrectable Pauli components (logical bit, phase, and joint bit-phase errors) generated across all pairs of errors $\{E_i, E_k\}$:

$$\Delta_{\text{QEC}}(t) = \sum_{i,k} \left\| M_{ik}(t) - \frac{1}{2} \text{Tr}[M_{ik}(t)] P_C(t) \right\|_2, \quad (6)$$

where $\|\cdot\|_2$ denotes the 2-norm when applied to matrices, and the standard Euclidean norm when applied to vectors.

The state-dependent instantaneous leakage, $L_{\mathcal{E}_j, \psi_{E_j}}(t)$, measures the weight in states outside the target error manifold associated with a specific error E_j . For an initial state $|\psi_{E_j}\rangle \in \mathcal{E}_j(0)$, it is defined as the probability that the state, having undergone an error E_j , drifts outside the instantaneous error subspace $\mathcal{E}_j(t)$:

$$L_{\mathcal{E}_j, \psi_{E_j}}(t) = 1 - \text{Tr} \left[P_{\mathcal{E}_j}(t) \rho_{|\psi_{E_j}\rangle}(t) \right], \quad (7)$$

where $\rho_{|\psi_{E_j}\rangle}(t)$ is the density matrix at time t , when initialized as $\rho_{|\psi_{E_j}\rangle}(0) = |\psi_{E_j}\rangle\langle\psi_{E_j}|$ and evolved unitarily under the driven Hamiltonian without losses.

To assess the preservation of coherence within the subspace, we define the state-dependent trajectory mismatch, $\eta_{\mathcal{E}_j, \psi}(t)$. This metric quantifies the unitary rotation error by calculating the Euclidean distance between the Bloch vectors of the code state and the projected error state in the instantaneous subspaces:

$$\eta_{\mathcal{E}_j, \psi}(t) = \|\vec{r}_C(t) - \vec{r}_{E_j}(t)\|_2, \quad (8)$$

where the Bloch vectors are given by $\vec{r}_C(t) = \text{Tr}[\vec{\sigma}_C(t)\rho_{|\psi\rangle}(t)]$ and $\vec{r}_{E_j}(t) = \text{Tr}[\vec{\sigma}_{E_j}(t)\tilde{\rho}_{|\psi_{E_j}\rangle}(t)]$. Here, $\vec{\sigma}_C(t)$ and $\vec{\sigma}_{E_j}(t) \propto E_j \vec{\sigma}_C(t) E_j^\dagger$ are vectors of the logical Pauli operators in the instantaneous code and error subspaces. The density matrices $\rho_{|\psi\rangle}(0)$ and $\rho_{|\psi_{E_j}\rangle}(0)$ are initialized as a pure logical state $|\psi\rangle \in \mathcal{C}(0)$ and the

corresponding error space state $|\psi_{E_j}\rangle \propto E_j|\psi\rangle$, respectively. After the unitary evolution by the system Hamiltonian and Schrodinger equation, the evolved states are projected onto the instantaneous code and error spaces, respectively, and normalized to obtain $\tilde{\rho}_{|\psi\rangle}$ and $\tilde{\rho}_{|\psi_{E_j}\rangle}(t)$ (note that $\tilde{\rho}_{|\psi\rangle}(t) = \rho_{|\psi\rangle}(t)$ by definition of instantaneous code space).

These three metrics quantify deviations from error-transparent evolution, with optimal performance achieved as each approaches zero. A vanishing QEC violation, $\Delta_{\text{QEC}}(t) = 0$, ensures the evolving code words remain correctable throughout the operation. A vanishing leakage, $L_{\mathcal{E}_j, \psi_{E_j}}(t) = 0$ for all $|\psi_{E_j}\rangle \in \mathcal{E}_j(0)$, implies the evolving error space and instantaneous error space coincide. Finally, a vanishing trajectory mismatch, $\eta_{\mathcal{E}_j, \psi}(t) = 0$ for all $|\psi\rangle \in \mathcal{C}(0)$, indicates that the instantaneous error subspace evolution is identical to the code subspace evolution throughout the gate operation. These three metrics being simultaneously satisfied at all times t and for all logical (error) states $|\psi\rangle$ ($|\psi_{E_j}\rangle$) ensures the evolution satisfies the condition for dynamic error transparency.

III. APPLICATION TO A BINOMIAL CODE

We now turn to applying this concept to bosonic codes, specifically the binomial ‘kitten’ code. To realize such EsT operations leveraging a dynamic subspace framework, we encode a logical qubit in a superconducting cavity (harmonic oscillator), dispersively coupled to a transmon qubit ancilla [30] as shown in Fig. 1c. The system Hamiltonian at low order is given by:

$$H/\hbar = \omega_a \hat{a}^\dagger \hat{a} + \omega_q \hat{q}^\dagger \hat{q} + \chi \hat{a}^\dagger \hat{a} \hat{q}^\dagger \hat{q} + \frac{K_a}{2} \hat{a}^{\dagger 2} \hat{a}^2 + \frac{K_q}{2} \hat{q}^{\dagger 2} \hat{q}^2 \quad (9)$$

where \hat{a} and \hat{q} are the annihilation operators for the cavity and transmon respectively, $\chi/2\pi = -3.66$ MHz is the dispersive coupling of the transmon and cavity, $K_a/2\pi = -22$ kHz is the self-Kerr of the cavity, $K_q/2\pi = -329$ MHz is the self-Kerr of the qubit (App. B describes details of experimental package). The cavity has $T_1 = 180 \mu\text{s}$ and $T_2 = 290 \mu\text{s}$ whereas the ancilla transmon has $T_1 = 70 \mu\text{s}$ and $T_2 = 30 \mu\text{s}$. This is the same package as used in Roy, *et al* [23].

In the cavity, we encode the binomial ‘kitten’ code [31, 32], which allows correction of single photon loss errors in the cavity. The codespace for this binomial code is defined on the even parity subspace as $\mathcal{C} = \text{span}\{|0_L\rangle, |1_L\rangle\}$, where $|0_L\rangle = \frac{|0\rangle + |4\rangle}{\sqrt{2}}$, $|1_L\rangle = |2\rangle$ are the two logical codewords. When a single photon loss error happens in the cavity, the logical state jumps into the orthogonal odd parity error space $\mathcal{E} = \text{span}\{|0_E\rangle, |1_E\rangle\}$, where $|0_E\rangle = |3\rangle$, $|1_E\rangle = |1\rangle$ are the two error words.

The flexibility of dynamic subspaces allows for the use of simpler linear drives that traverse trajectories outside this static code and error spaces to achieve fast, non-adiabatic operations while optimizing for ET (Fig. 1b)

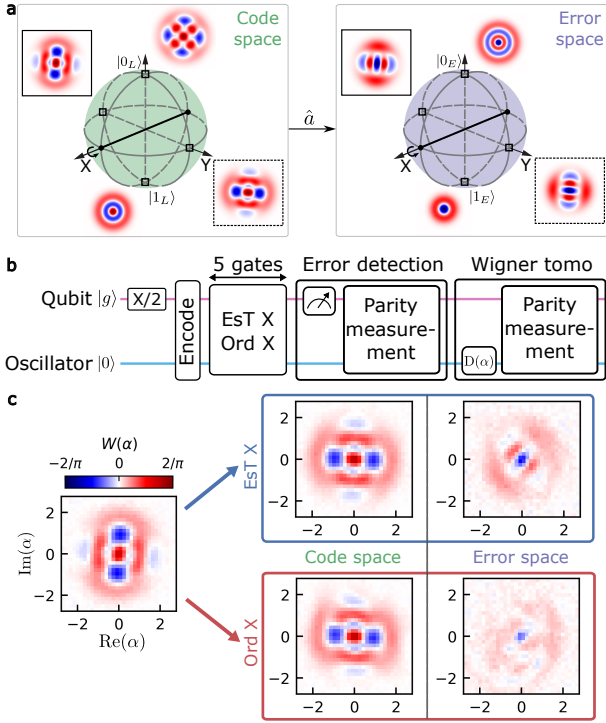


FIG. 2. Wigner visualization of error transparency: (a) Logical Bloch sphere of code space (left) and error space (right) corresponding to single photon loss errors in the oscillator for binomial ‘kitten’ code. The cardinal points and their theoretical Wigner functions are marked on the Bloch sphere. Starting from the state $| -Y_L\rangle = (|0_L\rangle - i|1_L\rangle)/\sqrt{2}$ (Wigner function in solid square box), a logical X operation is performed along the X axis (marked black) to end in the state $| +Y_L\rangle = (|0_L\rangle + i|1_L\rangle)/\sqrt{2}$ (Wigner function in dashed square box). (b) Experimental pulse sequence for characterizing EsT gates. After the gate operation, we read out the qubit state and measure the parity of the oscillator state to detect errors and perform Wigner tomography. Based on this parity measurement, we post-process the Wigner functions of states in code and error space. (c) Experimentally measured Wigner functions of binomial code cardinal point $| -Y_L\rangle = (|0_L\rangle - i|1_L\rangle)/\sqrt{2}$ and the state after applying five EsT or Ord X gates are shown. Left side plots of code space Wigner function is conditioned on detection of no error ($\sim 90\%$ of shots) and shows similar performance for EsT and Ord gate. Right side plot of error space Wigner function is conditioned on detection of single photon loss error ($\sim 10\%$) and shows EsT gate significantly preserves the phase coherence and state amplitudes of the target state compared to Ord gate. Error space Wigners have a fixed global frame rotation compared to code space because of qubit being in excited state for longer during the measurement.

through the gate. We consider the drive Hamiltonian

$$H_{\text{drive}}(t)/\hbar = \epsilon(t)\hat{a} + \Omega(t)\hat{q} + \text{h.c.} \quad (10)$$

However, evolutions of the codespace under linear drive on the oscillator does not generically commute with photon loss operator \hat{a} , the primary loss channel for the binomial code \mathcal{C} , on the codespace. Consequently, exact ET is not

expected to be achieved in this setup, but trading exactness for a simpler and more scalable experimental setup may offer practical advantage and higher experimental fidelities by improving reliability and reducing spurious error channels. We refer to operations that deviate from exact error transparency as error semi-transparent (EsT) [33].

We construct the target EsT unitary by numerically engineering the time-dependent drive Hamiltonian ($H_{\text{drive}}(t)$). We optimize complex drive amplitudes simultaneously applied on the cavity ($\epsilon(t)$) and the ancilla qubit ($\Omega(t)$) (Fig. 1c), using GRAPE [24, 25, 34] for accomplishing logical X, H, and T gates on the binomial code. The Ord gates are optimized with the single objective of obtaining highest fidelity operation in the code space. For EsT gates, an appropriately weighted objective of error transparency (see eqn. C7, C8) is added in addition to obtaining high fidelity operation in code and error subspaces. To facilitate differentiability, we utilize a cost function based on state overlaps and fidelities rather than commutator norms and projectors for defining error transparency. Further details of the numerical optimization is described in App. C. Logical X and H gates are implemented with a duration of $1\ \mu\text{s}$ with simultaneous qubit and cavity drives, while the T gate is realized with only qubit drives in $0.6\ \mu\text{s}$. To appropriately compare the performance of EsT and Ord gates, we select pulses that reach the same maximum active Fock state ($|11\rangle$ for X and H gates), defined as the highest Fock state $|n\rangle$ to achieve a transient probability of occupation greater than 0.01.

IV. RESULTS

We simulate the dynamics of the oscillator under the Ord and EsT gates and calculate the violation metrics defined in Eqn. 6-8. We observe the optimization for EsT gate successfully minimizes violation of the QEC conditions in the instantaneous code space, reducing leakage out of the instantaneous error space due to photon loss, and enforcing trajectory and coherence matching in the instantaneous code and error spaces. The Ord gate has no such constraint and therefore exhibits substantial QEC violation, leakage and trajectory mismatch due to photon loss. We compare the QEC violation, leakage of the evolved error space out of the instantaneous error space during the operation and the trajectory mismatch in Fig. 1d-e respectively. Leakage and trajectory mismatches are plotted for evolution of initial states $|0_E\rangle$ and $|0_L\rangle$ respectively. Values closer to zero suggest a lower violation of the instantaneous conditions required to satisfy ET. These plots confirm how the optimizer enables the pulse to be EsT.

While these metrics quantify ET at a specific moment, the final gate fidelity will depend on both the immediate impact of the error and the subsequent evolution under the remaining control pulse. To capture this full effect,

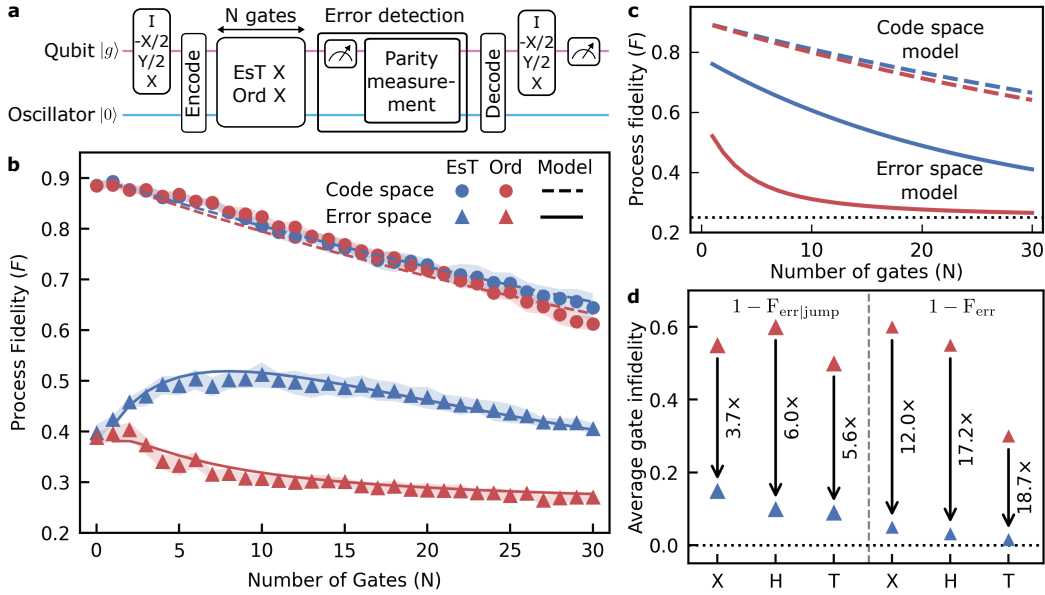


FIG. 3. Code and error space process tomography: (a) Experimental pulse sequence to perform code and error space process tomography. Following the gate operations, we perform qubit readout and oscillator parity measurement for error detection based on which we post-select our states into code and error space. Separate decode operations are used that respectively maps the code and error space states to the ancilla qubit state for performing process tomography. (b) Experimentally measured code (dots) and error space (triangles) process fidelities for EsT and Ord X gate with number of applied gates are shown (see App. C for details). Shaded region around the data points signify 1 standard deviation of measured fidelities in repeated experiments. Dashed lines for code space and solid lines for error space show modeled gate performance with number of gates. In codespace, both gates perform similarly while in the error space EsT gate performs significantly better than the Ord gate. The horizontal dashed line at process fidelity of 0.25 indicates a completely incoherent process. (c) We plot the modeled code and error space process fidelities without non-idealities of the error detection process. This shows a clear difference in error space process fidelity of EsT and Ord gates. (d) We summarize the infidelities for X , H and T gates extracted from our model for (left side of plot) error during the operation that takes a state from code space to error space ($1 - F_{\text{err|jump}}$) and (right side of plot) operations in the error space ($1 - F_{\text{err}}$). Factor of reduction in infidelity is marked by the arrow for all the cases.

we can evaluate the gate fidelity conditioned on a single photon loss event occurring at an arbitrary time during the operation. As detailed in App. D, the EsT gate maintains a higher conditional fidelity across the pulse duration compared to Ord gate.

To verify the ET property, we performed Wigner tomography on the states following the application of 5 X gates on the prepared state $|-Y_L\rangle = (|0_L\rangle - i|1_L\rangle)/\sqrt{2}$. Fig. 2a shows ideal Wigner functions of initial (solid box) and final state (dashed box) after application of X gate in the code and error space logical Bloch spheres. We show the pulse sequence for the experiment in Fig. 2b. After applying the gate, we read out the qubit state followed by parity measurement of the cavity state and finally perform Wigner tomography [35]. If there is a photon loss error during the operation, the state ends in the error subspace. Based on the parity measurement before the Wigner tomography, we post-select the final state in code and error subspaces. We show the measured Wigner functions for prepared $|-Y_L\rangle$ states and the states in code (left) and error (right) space after EsT and ord gates in Fig. 2c. Code and error space Wigners have different fixed global frame rotation due to qubit being in the excited state for longer during the parity measurement process, which can

be fixed with a frame rotation in software.

The Wigner functions measured in the codespace indicate that the X gate is accomplished and the logical states exhibit similar coherence within this subspace for both the EsT and Ord gates. Crucially, phase coherence and state amplitudes in the error space are preserved for the EsT gate, whereas they are significantly corrupted for the Ord gate.

We quantify the performance in the code and error space conditioned on single photon loss by performing quantum process tomography (QPT) [28, 36] of the states following the sequence shown in Fig. 3a and post-selecting on the code and error space states based on the parity measurement. Different decode operations are used that respectively map code and error space states to ancilla qubit states for extracting the fidelities in those subspaces. To focus only on the oscillator photon loss error to which the gate construction is EsT, we also post-select only the cases where the qubit is in the ground state at the end of the gate operations. Details of this analysis and further experimental data are given in App. E.

Experimentally measured fidelities for the code (circles) and error (triangles) space are shown for EsT and Ord X gates in Fig. 3b. To understand the dynamics and

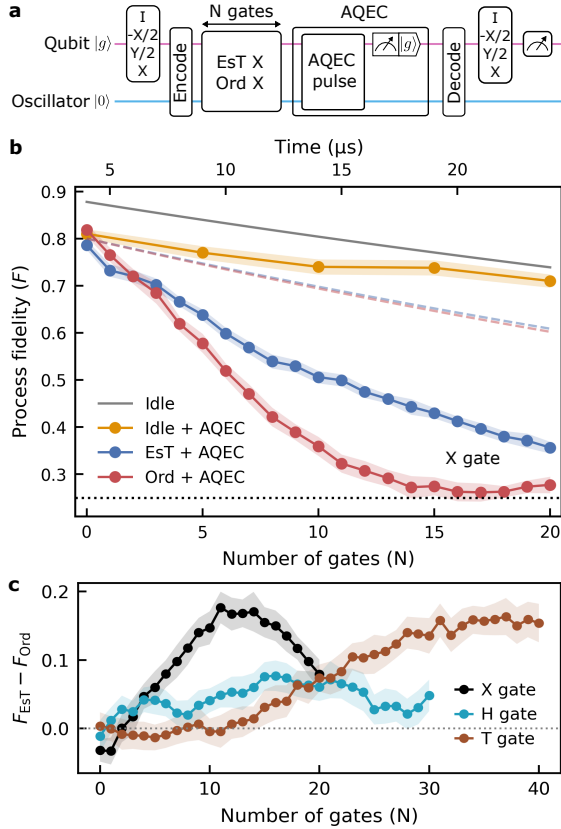


FIG. 4. **EsT gates protected by AQEC:** (a) Experimental sequence to check gate performance with AQEC. We perform a single AQEC step after N gates and perform process tomography. (b) We show the performance of EsT and Ord X gate with number of gates applied before doing error correction. EsT gate outperforms the Ord gate and the improvement increases with number of gates and then decreases as uncorrectable qubit errors, two photon loss errors in oscillator and control errors start to dominate. The plot also shows curves for process fidelity decay for idling and for applying an AQEC pulse after idling for an equivalent duration of N gates. The blue and red dashed lines provide a visual reference for simulated idling decay curves, calculated at an average photon number equal to the average photon number during the gate operation. The horizontal dashed line at process fidelity of 0.25 indicates a completely incoherent process and shaded regions around the data points signify 1 standard deviation of fidelities for repeated measurements. The top X axis shows the total duration of the experiment that includes encode, decode, AQEC pulse and active reset of qubit. (c) Summary of improvement in gate fidelity for EsT gate compared to Ord gate by applying AQEC as a function of the number of gates for X, H and T gates.

extract gate fidelities, we model the fidelity performance of the EsT and Ord gates as a function of the number of gates applied. The modeled curves, shown as dashed lines for code space and solid lines for error space, match our experimental data well. This plot confirms that the fidelity in code space is comparable for EsT and Ord gates, whereas in the error space, EsT gates exhibit substantially

higher fidelity compared to Ord gates.

The decay of error-space fidelity with gate depth appears non-intuitive at first glance. This is due to two processes that dominate over photon loss during the gates at short times (after only a few gates). The first is due to state preparation, which has an error that produces some weight in error subspaces. The second is that the parity measurement process itself has an error of $\sim 5\%$. So, at short times, a state selected in the error subspace has a small probability of being there as a result of photon loss during the gate. We model these error channels to fit the observed decay curves, allowing us to estimate the expected decay profiles free of parity selection errors. (see App. F for details). These ‘intrinsic’ fidelities of the gates are presented in Fig. 3c. This plot further validates the similarity in code space performance and the improvement in error space performance for EsT gates compared to Ord gates.

From the model that fits experimental data, we can extract the per-gate fidelity in case of a photon loss during the operation ($F_{\text{err}|j\text{ump}}$) and the fidelity of the operation in the error space (F_{err}). For X gate, $F_{\text{err}|j\text{ump}}$ increases from 0.45 to 0.85 and F_{err} increases from 0.4 to 0.95 for the EsT gate compared to Ord gate. We summarize these numbers in Fig. 3d for X, H and T gates. Averaged across the set of gates, we observe 5.1 times reduction in infidelity for the case of photon loss during the operation for the EsT gate compared to the Ord gate. This improvement is achieved because of the error transparency optimization. The per-gate infidelity in error space is reduced 16 times for the EsT gate. This improvement is because the Ord gate optimization does not optimize for the fidelity of operation in error space, whereas the EsT gate is optimized for that as well. This also raises the question whether optimizing for operation fidelity in both code and error subspaces is sufficient, without explicit error transparency optimization. To investigate this, we introduce the LE gate, where ‘LE’ stands for “Logical and Error space” gate. The LE gate maximizes operation fidelity in the code and error subspaces separately, but does *not* optimize for error transparency (see App. C for details of pulse construction). This gate shows intermediate performance that surpasses the Ord gate but remains inferior to the EsT gate. Additional experimental characterization and simulations are provided in App. E and App. D, respectively.

To demonstrate that the EsT gate performance improvement in error space remains valid after recovery to code space, we investigate the performance of gates under autonomous quantum error correction (AQEC) protection by applying the experimental sequence in Fig. 4a. The AQEC pulse is numerically optimized with a duration of $1\ \mu\text{s}$ to recover error states to code states and transfer the error entropy to the ancilla qubit (see App. C2). The ancilla qubit is then conditionally reset to the ground state, followed by a measurement which takes another $1.2\ \mu\text{s}$ [19]. We note that other AQEC methods have also been demonstrated in recent experiments, which can

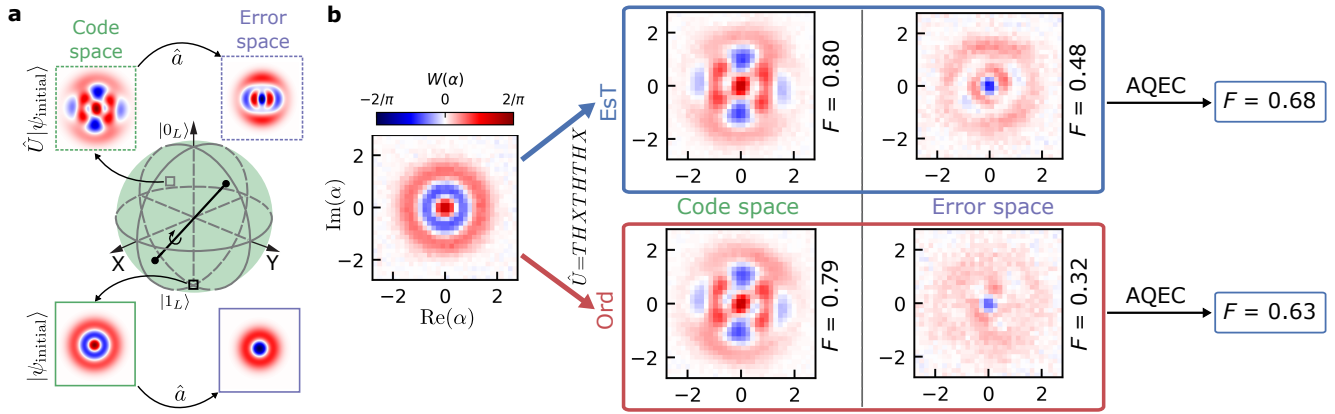


FIG. 5. **EsT protection for non-trivial sequence:** (a) Logical code space Bloch sphere showing the ideal Wigner functions before (solid box) and after (dashed) the non-trivial $THXTHTHX$ operation sequence that effectively rotates the state around the marked non-trivial rotation axis (black line). The ideal error space Wigner functions are also shown. (b) We show the experimentally measured Wigner functions of the prepared $|1_L\rangle$ state, the final state post-selected in code and error subspace after applying the pulse sequence comprising of EsT and Ord gates. We measure the process fidelities as reported on the side of the measured Wigner functions. Finally, we apply the AQEC pulse and measure the process fidelity. We observe a 0.05 improvement in process fidelity for the EsT gate sequence compared to the Ord gate sequence.

potentially perform better than this AQEC technique [8, 9, 37, 38]

As shown in Fig. 4a, we repeatedly applied N gates followed by a single AQEC step. Experimentally measured process fidelities for the EsT and Ord X gates are shown in Fig. 4b. As the gate depth N increases, the difference in process fidelity between the EsT and Ord gates widens. The improvement comes from both being EsT and better performance of the EsT gate in the error subspace. As the number of gates increases, uncorrectable two-photon loss errors in the oscillator, ancilla qubit errors and control errors start to dominate, reducing the performance improvement. Experimentally measured process fidelities for applying a single AQEC operation after waiting for a time equivalent to the gate operations are also plotted in Fig. 4b alongside a process fidelity decay curve for idling. These curves demonstrate that while our AQEC pulse lowers the absolute measured fidelity, it actively recovers quantum information from the error space and thereby slows the decay of encoded, actively manipulated quantum information in code space. We have also added red and blue dashed lines as a visual reference for simulated idling decay curves, calculated at an average photon number 2.1 equal to the average photon number during the gate operation.

We perform this experiment for H and T gates and summarize the improvement in fidelity for the EsTs gate compared to the Ord gates in Fig. 4c. For X and H gates, the fidelity improvement increases with the number of gates and then decreases due to the aforementioned reasons. For T gate, we see performance improvement up to 40 gates and expect it to decrease after that. We note here that EsT H gate has a lower fidelity improvement with AQEC even though it had better error space performance fidelities ($F_{\text{err|jump}}$ and F_{err} compared to the X gate. We

attribute this to the following two facts. Due to fluctuations of device parameters, EsT gate fidelity without the AQEC was lower for the H gate, and the probability of oscillator photon loss during the gate is higher for the H gate compared to the X gate (see App. E for details). This could be resolved in the future by engineering robustness objectives into the numerical optimization [39, 40]. Control errors mentioned above may also be mitigated by calibration of pulses with hardware feedback using reinforcement learning methods [41, 42].

Finally, we demonstrate that the EsT property is preserved when gates are concatenated by performing a non-trivial gate sequence ($THXTHTHX$) on a prepared $|1_L\rangle$ state. This gate does an effective clockwise rotation of 158 degrees around the rotation axis (0.47, 0.75, 0.47) as shown on the code space Bloch sphere in Fig. 5. Ideal Wigner functions of the initial state (solid box) and final state (dashed box) in code and error space are also shown. Fig. 5b shows the experimentally measured Wigner function of the prepared $|1_L\rangle$ state. After applying the gate sequence, following the protocol shown in Fig. 2b, we post-select our states in code and error spaces based on parity measurement and measure Wigner functions of states in those subspaces. Both gates perform the desired operation with similar fidelity in code space. In the error space, the EsT gate preserves the phase coherence and state amplitudes of the target state better than the Ord gate. Fidelities beside the Wigners are experimentally measured process fidelities in code and error subspaces. Upon applying AQEC, we recovered process fidelities of 0.68 and 0.63 respectively for EsT and Ord gate, representing a net fidelity improvement of 0.05 for the operation sequence.

We also simulate this sequence to understand the fidelities without SPAM and control errors, We get code space

fidelities of 0.94 and 0.92 for EsT and Ord gates sequence, respectively. In the error space conditioned on single photon loss of the oscillator, the EsT sequence achieves a fidelity of 0.82 compared to 0.35 for Ord sequence. This shows a 3.6 times reduction in infidelity in the error space. Following AQEc, the final fidelities are 0.86 for EsT and 0.82 for Ord sequence. This confirms that the optimized gates are mutually compatible, enabling synthesis of universal control over oscillator encodings with discrete EsT operations.

V. DISCUSSION AND OUTLOOK

In this work, we design an error semi-transparent (EsT) operation with simple linear drives leveraging dynamic subspaces to have universal control on a binomial bosonic logical qubit. We show that trading off exact ET for simpler control can enable substantial performance improvement for actively manipulated bosonic quantum information. Our design framework for EsT gates can be readily extended to other rotation-symmetric codes, such as four-legged cat codes [4, 43] and higher order binomial codes [31]. Our optimization framework also provides a pathway to explore the trade-offs for an approximate Eastin-Knill theorem [44] in standard qubit architectures and construction of fast, approximately bias-preserving operations for erasure qubits [45, 46].

However, because the linear drive does not commute with the photon loss operation on the codespace, an exactly ET operation is not likely to be achievable. In App. A, we describe further intuition for the limitations of the linear drive and comment on possible improvements. Improvements in ET performance can be obtained with optimization for additional objectives of minimizing mean photon number difference of evolving code words and leakage. An optimization involving dynamics obtained from solving the master equation, taking into account the loss rates of the system, will be able to account for the probability of photon jump and no-jump errors and therefore show further performance improvement. One could leverage dynamic subspace ET construction and obtain a theoretically exact ET with strong nonlinear drives (such as squeezing) using additional or different circuit elements. However, the utility of such schemes must be balanced with the increase in circuit and protocol complexity that potentially leads to more error channels.

The remaining dominant error source in the circuit is the decoherence of the transmon ancilla. Historically, the ancilla has had higher decoherence rates than the oscillator. However, due to the use of higher oscillator levels during a fast amplitude-mixing gate, the effective error probability during the gate is comparable for both the oscillator and the qubit as measured in experiments (App. E) and validated by simulations (App. D). In principle, qubit errors could be mitigated by replacing the qubit drives with a few simultaneous off-resonant Photon-Assisted Stark Shift (PASS) drives [19], optimizing their

amplitude to impart the necessary geometric phase to the cavity states without exciting the ancilla. However, this approach necessitates inefficiently long gate times to maintain adiabaticity or risks higher decoherence rates and ancilla population with stronger drives. Alternatively, a multi-level ancilla could be utilized to numerically enforce ancilla path independence alongside oscillator error transparency [17, 20, 47]. Utilizing the g - f transition of the ancilla for control would facilitate the detection of ancilla errors by monitoring the leakage to the state $|e\rangle$, thereby heralding ancilla errors [48, 49]. Such heralding of error is advantageous as it converts generic errors into erasure errors with known location.

In summary, we have introduced the concept of dynamic subspaces as a framework for realizing Error semi-transparent (EsT) operations. By traversing beyond static code and error spaces, this approach enables fast universal control of bosonic encodings using simpler linear drives. Our results demonstrate that EsT operations significantly enhance the fidelity of actively controlled bosonic qubits. Our approach is also compatible with methods for ancilla error detection [48, 49] offering a practical pathway towards error-mitigated universal control of bosonic quantum information.

ACKNOWLEDGMENTS

We acknowledge B. Cole, C. P. Larson, E. Yelton, B. L. T. Plourde, and Luojia Zhang for help in fabrication of the chip with the transmon and readout resonator and Chris Wang for design of the superconducting cavity. We thank Haoran Lu and Kushagra Aggarwal for their help with the cryogenic microwave setup. We also thank Maciej Olszewski and Xiangqin Wang for helpful discussions. We acknowledge helpful discussions and comments on the manuscript by Baptiste Royer. We also thank Sridhar Prabhu, Peter McMahon and Chen Wang for their remark on their manuscript.

This work was supported by the NSF under award number 2512537, as well as by the Aref and Manon Lahham Faculty Fellowship. We gratefully acknowledge Nord Quantique for the fabrication of the $\lambda/4$ superconducting cavity and MIT Lincoln Laboratory for supplying the Josephson traveling-wave parametric amplifier used in our experiments. This work was performed in part at the Cornell NanoScale Facility, a member of the National Nanotechnology Coordinated Infrastructure (NNCI), which is supported by the National Science Foundation (NSF) (Grant No. NNCI-2025233).

AI usage disclosure We have used Google Gemini 3 model strictly to assist with stylization and formatting of the figures only.

Author contributions S. R. and V. F. proposed the idea of using linear drives for EsT operation. S. R. developed the dynamic subspace EsT theory with O. C. W and V. F.. S. R. performed the numerical optimizations, experiments, and analysis. S. R. and V. F. wrote the

manuscript with input from O. C. W. V. F. supervised the project.

DATA AND CODE AVAILABILITY

Data and code that support the findings of this article are openly available in [10.5281/zenodo.18916619](https://doi.org/10.5281/zenodo.18916619).

- [1] R. Acharya, D. A. Abanin, L. Aghababaie-Beni, I. Aleiner, T. I. Andersen, M. Ansmann, F. Arute, K. Arya, A. Asfaw, N. Astrakhantsev, J. Atalaya, R. Babbush, D. Bacon, B. Ballard, J. C. Bardin, J. Bausch, A. Bengtsson, A. Bilmes, S. Blackwell, S. Boixo, G. Bortoli, A. Bourassa, J. Bovaird, L. Brill, M. Broughton, D. A. Browne, B. Buchea, B. B. Buckley, D. A. Buell, T. Burger, B. Burkett, N. Bushnell, A. Cabrera, J. Campero, H.-S. Chang, Y. Chen, Z. Chen, B. Chiaro, D. Chik, C. Chou, J. Claes, A. Y. Cleland, J. Cogan, R. Collins, P. Conner, W. Courtney, A. L. Crook, B. Curtin, S. Das, A. Davies, L. De Lorenzo, D. M. Debroy, S. Demura, M. Devoret, A. Di Paolo, P. Donohoe, I. Drozdov, A. Dunsworth, C. Earle, T. Edlich, A. Eickbusch, A. M. Elbag, M. Elzouka, C. Erickson, L. Faoro, E. Farhi, V. S. Ferreira, L. F. Burgos, E. Forati, A. G. Fowler, B. Foxen, S. Ganjam, G. Garcia, R. Gasca, É. Genois, W. Giang, C. Gidney, D. Gilboa, R. Gosula, A. G. Dau, D. Graumann, A. Greene, J. A. Gross, S. Habegger, J. Hall, M. C. Hamilton, M. Hansen, M. P. Harrigan, S. D. Harrington, F. J. H. Heras, S. Heslin, P. Heu, O. Higgott, G. Hill, J. Hilton, G. Holland, S. Hong, H.-Y. Huang, A. Huff, W. J. Huggins, L. B. Ioffe, S. V. Isakov, J. Iveland, E. Jeffrey, Z. Jiang, C. Jones, S. Jordan, C. Joshi, P. Juhas, D. Kafri, H. Kang, A. H. Karamlou, K. Kechedzhi, J. Kelly, T. Khairé, T. Khatrar, M. Khezri, S. Kim, P. V. Klimov, A. R. Klots, B. Kobrin, P. Kohli, A. N. Korotkov, F. Kostritsa, R. Kothari, B. Kozlovskii, J. M. Kreikebaum, V. D. Kurilovich, N. Lacroix, D. Landhuis, T. Lange-Dei, B. W. Langley, P. Laptev, K.-M. Lau, L. Le Guevel, J. Ledford, J. Lee, K. Lee, Y. D. Lensky, S. Leon, B. J. Lester, W. Y. Li, Y. Li, A. T. Lill, W. Liu, W. P. Livingston, A. Locharla, E. Lucero, D. Lundahl, A. Lunt, S. Madhuk, F. D. Malone, A. Maloney, S. Mandrà, J. Manyika, L. S. Martin, O. Martin, S. Martin, C. Maxfield, J. R. McClean, M. McEwen, S. Meeks, A. Megrant, X. Mi, K. C. Miao, A. Mieszala, R. Molavi, S. Molina, S. Montazeri, A. Morvan, R. Movassagh, W. Mruzckiewicz, O. Naaman, M. Neeley, C. Neill, A. Nersisyan, H. Neven, M. Newman, J. H. Ng, A. Nguyen, M. Nguyen, C.-H. Ni, M. Y. Niu, T. E. O’Brien, W. D. Oliver, A. Opremcak, K. Ottosson, A. Petukhov, A. Pizzuto, J. Platt, R. Potter, O. Pritchard, L. P. Pryadko, C. Quintana, G. Ramachandran, M. J. Reagor, J. Redding, D. M. Rhodes, G. Roberts, E. Rosenberg, E. Rosenfeld, P. Roushan, N. C. Rubin, N. Saei, D. Sank, K. Sankaragomathi, K. J. Satzinger, H. F. Schurkus, C. Schuster, A. W. Senior, M. J. Shearn, A. Shorter, N. Shutty, V. Shvarts, S. Singh, V. Sivak, J. Skruzny, S. Small, V. Smelyanskiy, W. C. Smith, R. D. Somma, S. Springer, G. Sterling, D. Strain, J. Suchard, A. Szasz, A. Sztein, D. Thor, A. Torres, M. M. Torunbalci, A. Vaishnav, J. Vargas, S. Vdovichev, G. Vidal, B. Villalonga, C. V. Heidweiller, S. Waltman, S. X. Wang, B. Ware, K. Weber, T. Weidel, T. White, K. Wong, B. W. K. Woo, C. Xing, Z. J. Yao, P. Yeh, B. Ying, J. Yoo, N. Yosri, G. Young, A. Zalcman, Y. Zhang, N. Zhu, N. Zobrist, G. Q. AI, and Collaborators, Quantum error correction below the surface code threshold, *Nature* **638**, 920 (2025).
- [2] R. Acharya, I. Aleiner, R. Allen, T. I. Andersen, M. Ansmann, F. Arute, K. Arya, A. Asfaw, J. Atalaya, R. Babbush, D. Bacon, J. C. Bardin, J. Basso, A. Bengtsson, S. Boixo, G. Bortoli, A. Bourassa, J. Bovaird, L. Brill, M. Broughton, B. B. Buckley, D. A. Buell, T. Burger, B. Burkett, N. Bushnell, Y. Chen, Z. Chen, B. Chiaro, J. Cogan, R. Collins, P. Conner, W. Courtney, A. L. Crook, B. Curtin, D. M. Debroy, A. Del Toro Barba, S. Demura, A. Dunsworth, D. Eppens, C. Erickson, L. Faoro, E. Farhi, R. Fatemi, L. Flores Burgos, E. Forati, A. G. Fowler, B. Foxen, W. Giang, C. Gidney, D. Gilboa, M. Giustina, A. Grajales Dau, J. A. Gross, S. Habegger, M. C. Hamilton, M. P. Harrigan, S. D. Harrington, O. Higgott, J. Hilton, M. Hoffmann, S. Hong, T. Huang, A. Huff, W. J. Huggins, L. B. Ioffe, S. V. Isakov, J. Iveland, E. Jeffrey, Z. Jiang, C. Jones, P. Juhas, D. Kafri, K. Kechedzhi, J. Kelly, T. Khatrar, M. Khezri, M. Kieferová, S. Kim, A. Kitaev, P. V. Klimov, A. R. Klots, A. N. Korotkov, F. Kostritsa, J. M. Kreikebaum, D. Landhuis, P. Laptev, K.-M. Lau, L. Laws, J. Lee, K. Lee, B. J. Lester, A. Lill, W. Liu, A. Locharla, E. Lucero, F. D. Malone, J. Marshall, O. Martin, J. R. McClean, T. McCourt, M. McEwen, A. Megrant, B. Meurer Costa, X. Mi, K. C. Miao, M. Mohseni, S. Montazeri, A. Morvan, E. Mount, W. Mruzckiewicz, O. Naaman, M. Neeley, C. Neill, A. Nersisyan, H. Neven, M. Newman, J. H. Ng, A. Nguyen, M. Nguyen, M. Y. Niu, T. E. O’Brien, A. Opremcak, J. Platt, A. Petukhov, R. Potter, L. P. Pryadko, C. Quintana, P. Roushan, N. C. Rubin, N. Saei, D. Sank, K. Sankaragomathi, K. J. Satzinger, H. F. Schurkus, C. Schuster, M. J. Shearn, A. Shorter, V. Shvarts, J. Skruzny, V. Smelyanskiy, W. C. Smith, G. Sterling, D. Strain, M. Szalay, A. Torres, G. Vidal, B. Villalonga, C. Vollgraff Heidweiller, T. White, C. Xing, Z. J. Yao, P. Yeh, J. Yoo, G. Young, A. Zalcman, Y. Zhang, N. Zhu, and G. Q. AI, Suppressing quantum errors by scaling a surface code logical qubit, *Nature* **614**, 676 (2023).
- [3] S. Krinner, N. Lacroix, A. Remm, A. Di Paolo, E. Genois, C. Leroux, C. Hellings, S. Lazar, F. Swiadek, J. Herrmann, G. J. Norris, C. K. Andersen, M. Müller, A. Blais, C. Eichler, and A. Wallraff, Realizing repeated quantum error correction in a distance-three surface code, *Nature* **605**, 669 (2022).
- [4] N. Ofek, A. Petrenko, R. Heeres, P. Reinhold, Z. Leghtas, B. Vlastakis, Y. Liu, L. Frunzio, S. M. Girvin, L. Jiang, M. Mirrahimi, M. H. Devoret, and R. J. Schoelkopf, Extending the lifetime of a quantum bit with error correction in superconducting circuits, *Nature* **536**, 441 (2016).
- [5] Z. Ni, S. Li, X. Deng, Y. Cai, L. Zhang, W. Wang, Z.-B. Yang, H. Yu, F. Yan, S. Liu, C.-L. Zou, L. Sun, S.-B. Zheng, Y. Xu, and D. Yu, Beating the break-even point with a discrete-variable-encoded logical qubit, *Nature* **616**, 56 (2023).
- [6] B. L. Brock, S. Singh, A. Eickbusch, V. V. Sivak, A. Z. Ding, L. Frunzio, S. M. Girvin, and M. H. Devoret, Quantum error correction of qudits beyond break-even, *Nature* **641**, 612 (2025).
- [7] V. V. Sivak, A. Eickbusch, B. Royer, S. Singh, I. Tsioutsios, S. Ganjam, A. Miano, B. L. Brock, A. Z. Ding, L. Frunzio, S. M. Girvin, R. J. Schoelkopf, and M. H. Devoret, Real-time quantum error correction beyond break-even, *Nature* **616**, 50 (2023).

- [8] L. Sun, Y. Xu, Y. Zhou, Z. Hua, W. Wang, J. Zhou, Z. jie Chen, L. Z. de Paula, Q.-X. Jie, G. Xue, H. Yu, W. Cai, C.-L. Zou, and L. Sun, Extending coherence time beyond break-even point using only drives and dissipation (2025), [arXiv:2509.22191](https://arxiv.org/abs/2509.22191).
- [9] S. Shirol, S. van Geldern, H. Xi, and C. Wang, Passive quantum error correction of photon loss at breakeven (2025), [arXiv:2510.19794](https://arxiv.org/abs/2510.19794).
- [10] L. Hu, Y. Ma, W. Cai, X. Mu, Y. Xu, W. Wang, Y. Wu, H. Wang, Y. P. Song, C.-L. Zou, S. M. Girvin, L.-M. Duan, and L. Sun, Quantum error correction and universal gate set operation on a binomial bosonic logical qubit, *Nature Physics* **15**, 503 (2019).
- [11] Y. Liu, S. Singh, K. C. Smith, E. Crane, J. M. Martyn, A. Eickbusch, A. Schuckert, R. D. Li, J. Sinanan-Singh, M. B. Soley, T. Tsunoda, I. L. Chuang, N. Wiebe, and S. M. Girvin, Hybrid oscillator-qubit quantum processors: Instruction set architectures, abstract machine models, and applications, *PRX Quantum* **7**, 010201 (2026).
- [12] W. Cai, Y. Ma, W. Wang, C.-L. Zou, and L. Sun, Bosonic quantum error correction codes in superconducting quantum circuits, *Fundamental Research* **1**, 50 (2021).
- [13] W.-L. Ma, S. Puri, R. J. Schoelkopf, M. H. Devoret, S. Girvin, and L. Jiang, Quantum control of bosonic modes with superconducting circuits, *Science Bulletin* **66**, 1789 (2021).
- [14] S. Bravyi and A. Kitaev, Universal quantum computation with ideal clifford gates and noisy ancillas, *Phys. Rev. A* **71**, 022316 (2005).
- [15] E. Kapit, Error-transparent quantum gates for small logical qubit architectures, *Phys. Rev. Lett.* **120**, 050503 (2018).
- [16] O. Vy, X. Wang, and K. Jacobs, Error-transparent evolution: the ability of multi-body interactions to bypass decoherence, *New Journal of Physics* **15**, 053002 (2013).
- [17] W.-L. Ma, M. Zhang, Y. Wong, K. Noh, S. Rosenblum, P. Reinhold, R. J. Schoelkopf, and L. Jiang, Path-independent quantum gates with noisy ancilla, *Phys. Rev. Lett.* **125**, 110503 (2020).
- [18] W.-L. Ma, S.-S. Li, and L. Jiang, Algebraic structure of path-independent quantum control, *Phys. Rev. Res.* **4**, 023102 (2022).
- [19] Y. Ma, Y. Xu, X. Mu, W. Cai, L. Hu, W. Wang, X. Pan, H. Wang, Y. P. Song, C.-L. Zou, and L. Sun, Error-transparent operations on a logical qubit protected by quantum error correction, *Nature Physics* **16**, 827 (2020).
- [20] P. Reinhold, S. Rosenblum, W.-L. Ma, L. Frunzio, L. Jiang, and R. J. Schoelkopf, Error-corrected gates on an encoded qubit, *Nature Physics* **16**, 822 (2020).
- [21] O. C. Wetherbee, S. Roy, B. Royer, and V. Fatemi, A Mathematical Structure for Amplitude-Mixing Error-Transparent Gates for Binomial Codes, *Quantum* **9**, 1890 (2025).
- [22] L. Bretheau, P. Campagne-Ibarcq, E. Flurin, F. Mallet, and B. Huard, Quantum dynamics of an electromagnetic mode that cannot contain n photons, *Science* **348**, 776 (2015), <https://www.science.org/doi/pdf/10.1126/science.1259345>.
- [23] S. Roy, A. Senanian, C. S. Wang, O. C. Wetherbee, L. Zhang, B. Cole, C. P. Larson, E. Yelton, K. Arora, P. L. McMahon, B. L. T. Plourde, B. Royer, and V. Fatemi, Synthetic high angular momentum spin dynamics in a microwave oscillator, *Phys. Rev. X* **15**, 021009 (2025).
- [24] R. W. Heeres, P. Reinhold, N. Ofek, L. Frunzio, L. Jiang, M. H. Devoret, and R. J. Schoelkopf, Implementing a universal gate set on a logical qubit encoded in an oscillator, *Nature Communications* **8**, 94 (2017).
- [25] S. Krastanov, V. V. Albert, C. Shen, C.-L. Zou, R. W. Heeres, B. Vlastakis, R. J. Schoelkopf, and L. Jiang, Universal control of an oscillator with dispersive coupling to a qubit, *Phys. Rev. A* **92**, 040303 (2015).
- [26] A. Eickbusch, V. Sivak, A. Z. Ding, S. S. Elder, S. R. Jha, J. Venkatraman, B. Royer, S. M. Girvin, R. J. Schoelkopf, and M. H. Devoret, Fast universal control of an oscillator with weak dispersive coupling to a qubit, *Nature Physics* **18**, 1464 (2022).
- [27] C. M. Dawson and M. A. Nielsen, The solovay-kitaev algorithm, *Quantum Info. Comput.* **6**, 81–95 (2006).
- [28] M. A. Nielsen and I. L. Chuang, *Quantum Computation and Quantum Information: 10th Anniversary Edition* (Cambridge University Press, Cambridge, 2010).
- [29] V. V. Albert, K. Noh, K. Duivenvoorden, D. J. Young, R. T. Brierley, P. Reinhold, C. Vuillot, L. Li, C. Shen, S. M. Girvin, B. M. Terhal, and L. Jiang, Performance and structure of single-mode bosonic codes, *Phys. Rev. A* **97**, 032346 (2018).
- [30] M. Reagor, W. Pfaff, C. Axline, R. W. Heeres, N. Ofek, K. Sliwa, E. Holland, C. Wang, J. Blumoff, K. Chou, M. J. Hatridge, L. Frunzio, M. H. Devoret, L. Jiang, and R. J. Schoelkopf, Quantum memory with millisecond coherence in circuit qed, *Phys. Rev. B* **94**, 014506 (2016).
- [31] M. H. Michael, M. Silveri, R. T. Brierley, V. V. Albert, J. Salmilehto, L. Jiang, and S. M. Girvin, New class of quantum error-correcting codes for a bosonic mode, *Phys. Rev. X* **6**, 031006 (2016).
- [32] A. L. Grimsmo, J. Combes, and B. Q. Baragiola, Quantum computing with rotation-symmetric bosonic codes, *Phys. Rev. X* **10**, 011058 (2020).
- [33] The terminology draws an optical analogy: because the dynamical evolutions within the code and error subspaces are not strictly identical, the operation acts as a semi-transparent one rather than a transparent one.
- [34] N. Khaneja, T. Reiss, C. Kehlet, T. Schulte-Herbrüggen, and S. J. Glaser, Optimal control of coupled spin dynamics: design of nmr pulse sequences by gradient ascent algorithms, *Journal of Magnetic Resonance* **172**, 296 (2005).
- [35] L. G. Lutterbach and L. Davidovich, Method for direct measurement of the wigner function in cavity qed and ion traps, *Phys. Rev. Lett.* **78**, 2547 (1997).
- [36] A. Hashim, L. B. Nguyen, N. Goss, B. Marinelli, R. K. Naik, T. Chistolini, J. Hines, J. Marceaux, Y. Kim, P. Gokhale, T. Tomesh, S. Chen, L. Jiang, S. Ferracin, K. Rudinger, T. Proctor, K. C. Young, I. Siddiqi, and R. Blume-Kohout, Practical introduction to benchmarking and characterization of quantum computers, *PRX Quantum* **6**, 030202 (2025).
- [37] J. M. Gertler, B. Baker, J. Li, S. Shirol, J. Koch, and C. Wang, Protecting a bosonic qubit with autonomous quantum error correction, *Nature* **590**, 243 (2021).
- [38] Z. Ni, L. Hu, Y. Cai, L. Zhang, J. Mai, X. Deng, P. Zheng, S. Liu, S.-B. Zheng, Y. Xu, and D. Yu, Autonomous quantum error correction beyond break-even and its metrological application (2025), [arXiv:2509.26042](https://arxiv.org/abs/2509.26042).
- [39] T. Propson, B. E. Jackson, J. Koch, Z. Manchester, and D. I. Schuster, Robust quantum optimal control with trajectory optimization, *Phys. Rev. Appl.* **17**, 014036 (2022).

- (2022).
- [40] P. M. Poggi, G. De Chiara, S. Campbell, and A. Kiely, Universally robust quantum control, *Phys. Rev. Lett.* **132**, 193801 (2024).
- [41] V. V. Sivak, A. Eickbusch, H. Liu, B. Royer, I. Tsioutsios, and M. H. Devoret, Model-free quantum control with reinforcement learning, *Phys. Rev. X* **12**, 011059 (2022).
- [42] Y. Baum, M. Amico, S. Howell, M. Hush, M. Liuzzi, P. Mundada, T. Merkh, A. R. Carvalho, and M. J. Biercuk, Experimental deep reinforcement learning for error-robust gate-set design on a superconducting quantum computer, *PRX Quantum* **2**, 040324 (2021).
- [43] M. Mirrahimi, Z. Leghtas, V. V. Albert, S. Touzard, R. J. Schoelkopf, L. Jiang, and M. H. Devoret, Dynamically protected cat-qubits: a new paradigm for universal quantum computation, *New Journal of Physics* **16**, 045014 (2014).
- [44] P. Faist, S. Nezami, V. V. Albert, G. Salton, F. Pastawski, P. Hayden, and J. Preskill, Continuous symmetries and approximate quantum error correction, *Phys. Rev. X* **10**, 041018 (2020).
- [45] A. Kubica, A. Haim, Y. Vaknin, H. Levine, F. Brandão, and A. Retzker, Erasure qubits: Overcoming the T_1 limit in superconducting circuits, *Phys. Rev. X* **13**, 041022 (2023).
- [46] S. Gu, A. Retzker, and A. Kubica, Fault-tolerant quantum architectures based on erasure qubits, *Phys. Rev. Res.* **7**, 013249 (2025).
- [47] Q. Xu, P. Zeng, D. Xu, and L. Jiang, Fault-tolerant operation of bosonic qubits with discrete-variable ancillae, *Phys. Rev. X* **14**, 031016 (2024).
- [48] T. Tsunoda, J. D. Teoh, W. D. Kalfus, S. J. de Graaf, B. J. Chapman, J. C. Curtis, N. Thakur, S. M. Girvin, and R. J. Schoelkopf, Error-detectable bosonic entangling gates with a noisy ancilla, *PRX Quantum* **4**, 020354 (2023).
- [49] W. Cai, Z.-J. Chen, M. Li, Q.-X. Jie, X.-B. Zou, G.-C. Guo, L. Sun, and C.-L. Zou, Error-detectable universal control for high-gain bosonic quantum error correction (2026), [arXiv:2601.21838](https://arxiv.org/abs/2601.21838).